EXPERIMENTAL AND NUMERICAL STUDY OF MOLECULAR ROTATIONAL DIFFUSION IN GEL-LIKE MEDIA

by

Ivan Lode André Maria Claeys

Research report submitted in partial fulfillment
of the requirements for admission to the degree
of Master of Science

Department of Chemical Engineering
California Institute of Technology
Pasadena, California 91125

26 April 1988

ACKNOWLEDGEMENTS

This report summarizes most of the research I did during the past year and a half. It has been an interesting and exciting project. I am deeply endebted to my research advisors, professors F.H. Arnold and J.F. Brady, for making it possible and for their optimism, support and insightful guidance during the most difficult moments of this venture. I am looking forward to what lies ahead.

I should also like to take this opportunity to thank the many friends I have found at Caltech. I hope that I shall keep enjoying their good company during the years to come, and I wish them good luck with their research.

Finally, I want to express my gratitude to my parents, and to Mariana, for being so understanding and for encouraging me to take on graduate studies at Caltech. Thank you very, very much.

Ivan.

ABSTRACT

The hindered rotational diffusion of biopolymers in porous or fibrous media plays a significant role in many industrial and natural processes. Nuclear magnetic relaxation experiments can be used to investigate how the gel matrix impedes the tumbling of molecules trapped in its pores. Indeed, molecular motions influence the relaxation rate by causing fluctuations of the local magnetic field experienced by the nuclear spins. Hence a measurement of relaxation times allows one to monitor the rotational diffusion of rigid molecules in gels and to detect matrix-induced anisotropic behavior. Experiments examining the ^{31}P relaxation of cGMP trapped in polyacrylamide gels showed more than a threefold decrease in the rotational diffusion coefficient when the gel concentration was brought from zero to 30%. Similar experiments in agarose gels prove that nuclear magnetic relaxation measurements can effectively be used to extract valuable information about rotational diffusion inside gels.

A Stokesian dynamics simulation of molecular diffusion in fibrous environments will complement the experimental studies. The mobility interactions between prolate spheroids in low Reynolds number linear flows have been derived. The expressions are exact at the level of forces, torques and stresslets, and the results are cast in a form suitable for numerical calculations. This extension of Stokesian dynamics to non-spherical particles forms the groundwork for computationally efficient, hydrodynamically accurate simulations of suspensions of rodlike particles.

TABLE OF CONTENTS

LIST OF FIGURES

1. Introduction

The rotational diffusion of a molecule trapped in a gel is of considerable importance in a great variety of processes. It determines the rate at which a rodlike polymer can reorient itself to squeeze through a maze of fibers, as in electrophoresis or size-exclusion chromatography. The rotational diffusion coefficient can also influence the overall kinetics of many biochemical reactions, since the presence of an active site makes the speed of conversion dependent on molecular orientation. This can reduce the effective turnover rate of an enzyme by several orders of magnitude if the diffusive approach of the reactants forms the limiting step in the reaction sequence.[1] Therefore, an understanding of molecular rotations in fibrous environments is essential for evaluating the overall kinetics of enzymatic reactions and for modeling processes such as affinity chromatography and some immobilization techniques. The gel-like structure of many organs also suggests biomedical applications, such as drug delivery in the eye or in connective tissue.

Unfortunately, the rotational diffusion coefficient cannot be measured by techniques commonly used to evaluate translational diffusion. Spectroscopy, however, can probe the microscopic details of molecular reorientation. In a shear flow, the dynamic balance between the hydrodynamic torque acting on a particle and its rotational Brownian motions results in an anisotropic distribution of molecular orientations. Linear dichroism and linear birefringence can detect this anisotropy. The former technique is based on the difference in extinction coefficients for polarized light along different molecular axes ; the latter exploits the orientation dependence of the refractive index. When the shear flow is suddenly stopped, rotary diffusion randomizes the orientations of the molecules. The rate at which the linear dichroism or the birefringence decay can then be related to the rotational diffusion coefficient.[2]

Laser light scattering experiments measure rotational diffusion in solution without perturbing the equilibrium distribution of orientations. Molecular motions modulate the fluctuations in the polarizability of the scattering medium, and hence influence the spectrum of the scattered light.[3] The contributions of the translational motion to the spectral width can be separated from the rotational effects by observing both the depolarized and the polarized components of the scattered light.[3] Neutron scattering samples motional fluctuations of much smaller amplitude (with a magnitude comparable to the wavelength of the irradiating beam, of the order of angstroms). These motions, however, are usually too rapid to be described by a diffusion equation.[3]

The infrared and Raman spectra of liquid methane, carbon monoxide and other small molecules have been interpreted in terms of molecular reorientations,[4,5] but their application to the study of macromolecular rotational diffusion is limited by the dominant contribution of vibrational modes and internal motion in larger molecules.[4] Fluorescence depolarization on the other hand is a very powerful tool. Following a pulse of plane polarized light, the fluorescence anisotropy decays as a result of rotative Brownian motions, which randomize the orientation of the excited chromophores. Evidently, information about the rotational diffusion can be extracted from such time resolved experiments. However, if the chromophore is flexibly bonded to the molecule of interest, or if there are several chromophores attached with different orientations to the same macromolecule, fluorescence depolarization will determine only a lower bound to the macromolecular reorientation times.[6]

The line shapes in electron paramagnetic resonance (EPR) provide detailed information about molecular rotational diffusion too,[7] but these analyses are restricted to free radicals or to molecules which can be appropriately spin-labeled. Last but not least, nuclear magnetic relaxation experiments have successfully been used to study molecular motions in solution and in solids.[8,9] These measurements are sensitive to both the rate and the geometry of the motions.[10,11] Moreover, since

the excitation frequency lies in the radiofrequency range, nuclear magnetic resonance (NMR) can be used to examine the rotational diffusion of molecules trapped in optically opaque gels, which are inaccessible to many other spectroscopic techniques such as fluorescence depolarization.

When a molecule undergoing Brownian motion is trapped inside a gel, its dynamics are affected in two ways (fig.1). First, the viscous interactions between the fibers and the molecule, transmitted through the solvent, will increase the friction factor of the particle. The link between the diffusion coefficient and the hydrodynamic properties of a small suspended object was first recognized by Einstein in his classic treatise on Brownian motion.[12] In 1906, he proposed that $D = kT/\Xi$, where D is the translational diffusion coefficient, k represents Boltzmann's constant, T is the absolute temperature and Ξ is the friction factor. ($\Xi = 6\pi\mu a$ for spherical particles according to Stokes' formula. μ stands for the viscosity of the fluid and a is the particle radius.) This relation was later verified experimentally by Perrin,[13] who extended it to include rotational motion and non-spherical molecules. In general then, for a particle of arbitrary shape, the diffusion tensor $\mathbf{D}$ is proportional to the mobility tensor $\mathbf{M}$ of the body.[14] This assumes that the particle Reynolds number is small. Hence viscous forces, rather than inertial effects, dominate the behavior of the solvent. Most molecules are small enough to satisfy this criterion, and many are large enough to legitimate the use of a continuum description for the solvent. From the Stokes-Einstein relation, or its generalization $\mathbf{D} = kT\,\mathbf{M}$, it is apparent that an increase in the hydrodynamic resistance of the molecule due to entrapment will decrease the diffusion coefficient. Because of the long-ranged character of hydrodynamic effects at low Reynolds numbers,[15] this viscous effect will be experienced even if the molecule is much smaller than typical pores in the gel. If the particle has dimensions comparable to the mean void space in the gel matrix, the diffusion tensor will be affected in an additional, more qualitative manner (fig.1c). The network of polymer chains will hinder some modes of motion more than others, causing anisotropic diffusive behavior. For example, in the case of a

prolate molecule, spinning around the azimuthal axis will be slowed, but rotation around the minor axis will become virtually impossible ; thus, entrapment in a gel amplifies the anisotropy of the molecular shape. Because of the dependence of nuclear magnetic relaxation on the rate and the geometry of motions, both effects can be investigated by fairly conventional NMR experiments.

2. Experimental Section

2.1 Principles of Nuclear Magnetic Relaxation

The concept that links nuclear spin relaxation to molecular dynamics is straightforward. When a molecule is placed in a magnetic field, the spontaneous alignment of the nuclear spins parallel or antiparallel to the applied field results in a net macroscopic magnetization. At equilibrium, the distribution of the spins among these two energy levels follows the Boltzmann law. In an inversion recovery experiment, the magnetic moment induced in the sample is inverted by a radiofrequency pulse and its return to equilibrium is monitored (fig.2). In most cases, the magnetization approaches its asymptotic value exponentially, with a time constant T_1.

This relaxation behavior reflects the motion of the molecule, and it is this relation that allows the investigation of molecular dynamics by NMR. The key concept is that the magnetic field experienced by a nuclear spin depends on its local environment, which changes as the molecule tumbles. For example, the electron cloud surrounding the nucleus effectively forms a shield against electromagnetic radiation. Since the electronic distribution in a molecule is non-uniform, this screening effect depends on the orientation of the molecule in the applied magnetic field (fig.3a). This is known as chemical shift anisotropy in the NMR literature. As a result of the anisotropic screening, rotational Brownian motion will modulate the effective field experienced by the nucleus. If these fluctuations match the Bohr relation, $\Delta E = h\nu$, they can induce transitions between the energy levels and lead to relaxation, i.e. a return to the equilibrium distribution. ΔE is the energy difference between the spin states, h is Planck's constant and ν is the frequency of the magnetic fluctuation. Hence a relaxation experiment actually samples the component of the molecular

motion at the Bohr frequency.

Other interactions can contribute to variations of the local magnetic field with orientation. A very important relaxation mechanism is the magnetic dipole-dipole interaction between nuclei (fig.3b). Each spin acts as a tiny dipole and generates its own lines of induction. Again the field experienced at one site depends on the position of the interacting spin, and hence on the orientation of the molecule relative to the applied magnetic field.

Quantitative expressions for the relaxation rates due to these mechanisms have been derived from time-dependent perturbation theory. In this treatment, the relevant interaction is treated as a small perturbation of the Hamiltonian describing the evolution of the spin system. The problem can then be handled using the formalism developed in Abragam's classic work on nuclear magnetism.[16] The relaxation time can be deduced ; for chemical shift anisotropy the formula reads :

$$\frac{1}{T_1^I} = \frac{2}{15}(\gamma_I B_0 \Delta\sigma)^2(1+\frac{\eta^2}{3})J_2^1(\omega_I) \qquad (1)$$

where γ_I is the gyromagnetic ratio of spin I,

B_0 is the applied magnetic field strength,

$\Delta\sigma$ and η characterize the chemical shift anisotropy,

ω_I is the transition frequency for spin I,

and $J(\omega)$ is the spectral density for the motion (see below).

For dipole-dipole interaction between the spins I and S, the expression is :

$$\frac{1}{T_1^I} = \frac{1}{5}\frac{\gamma_I^2\gamma_S^2\hbar^2}{r^6}S(S+1)\left\{\frac{1}{3}J_2^0(\omega_I-\omega_S)+J_2^1(\omega_I)+2J_2^2(\omega_I+\omega_S)\right\} \qquad (2)$$

where $\hbar$ is Planck's constant divided by 2π, and S is the spin quantum number of nucleus S. Besides the molecular geometry and the magnetic characteristics of the spin system, these expressions involve the "spectral density" $J_2^m(\omega)$. This function forms the link between molecular motions and the magnetic relaxation. $J_2^m(\omega)$ is the Fourier transform of an autocorrelation function for the orientation of the

molecule. By definition,

$$J_2^m(\omega) = \frac{1}{2}\int_{-\infty}^{+\infty} \left\langle Y_2^{-m}(\mathbf{\Omega}(0)) Y_2^m(\mathbf{\Omega}(t)) \right\rangle e^{-i\omega t}\, dt \tag{3}$$

where Y_2^m is a generalized spherical harmonic and $\mathbf{\Omega}(t)$ represents the set of angles needed to characterize the position of the molecule at time t. The angular brackets denote an ensemble average. The orientation $\mathbf{\Omega}(t)$ is obtained from the initial set of angles $\mathbf{\Omega}(0)$ by solving the appropriate model for molecular reorientation. In most cases, diffusive behavior may be assumed, and the equations derived by Favro for rotational Brownian motion apply.[17,18] The problem of coupled translational and rotational motions is examined by Brenner.[14] In the case of isotropic rotational diffusion (characterized by a single coefficient), i.e. when the molecular shape is adequately approximated as a sphere, the correlation function decays exponentially and the spectral density takes the form :

$$J_2^m(\omega) = \frac{6\, D_r}{(6D_r)^2 + \omega^2} \tag{4}$$

where D_r is the rotational diffusion coefficient. In the more general case where different coefficients characterize the diffusion about each of the principle axes, the autocorrelation function $\left\langle Y_2^{-m}(\mathbf{\Omega}(0)) Y_2^m(\mathbf{\Omega}(t)) \right\rangle$ consists of five exponentials.[19] The Fourier transformation then yields a sum of Lorentzians which depend on the eigenvalues D_x, D_y and D_z of the diffusion tensor. For symmetric tops, only three terms involving $D_{\|}$ and $D_{\perp}$ are retained.[20]

Typically, the relaxation time T_1 varies with the diffusion coefficient of the tumbling molecule as shown in fig.4 . The distinction between oblate and prolate bodies in this figure results from the dependence of the spectral density on $D_{\|}$ and $D_{\perp}$ and explains how anisotropic diffusion can be studied by NMR. For small molecules in solution, the rotational diffusion coefficient normally falls in the range $10^8\,\mathrm{s}^{-1}$ to $10^{11}\,\mathrm{s}^{-1}$. At the magnetic field strengths usually accessible, this motion is sufficiently rapid compared to the transition frequency to observe a direct proportionality between the relaxation time and the diffusion coefficient. Indeed,

in the extreme narrowing limit, i.e. for $6D_r >> \omega_I$, $J_2^m(\omega_I)$ reduces to $(6D_r)^{-1}$ (generally known as the rotational correlation time τ_c). In the presence of a fibrous matrix, molecular tumbling will be slowed, decreasing the rotational diffusion coefficient, and thus affecting the relaxation time. Both macroscopic quantities reflect the same microscopic phenomenon : rotational Brownian motion.

2.2 Materials and Methods

All samples were prepared using 50 mM solutions of cyclic guanosine monophosphate (cGMP ; M_W = 344) buffered at pH = 7.5. Either NN'methylene bisacrylamide (Bis) or NN'bisacryloylcystamine (BAC) was added as a crosslinker in polyacrylamide at a concentration of 4% (relative to the total acrylamide content). The samples were degassed under vacuum and polymerization occurred at room temperature[21] upon addition of 1 μl/ml of a freshly made 40% ammoniumpersulfate solution and 0.3 μl/ml of N,N,N',N' tetramethylethylenediamine (TEMED) under N_2 atmosphere. The longitudinal relaxation time T_1 of the single phosphorus atom in cGMP was measured by the inversion recovery technique at a Larmor frequency of 81 MHz (200 MHz proton frequency).

2.3 Experimental Results and Discussion

We performed several experiments monitoring the phosphorus relaxation of cGMP trapped in various types of gels. The results for several concentrations of polyacrylamide are shown in fig.5. As expected, the relaxation time decreases with increasing gel concentration. Assuming extreme narrowing, the relaxation time is a direct measure of the effective rotational diffusion coefficient. Hence we observed more than a threefold decrease in the diffusion of cGMP when the gel concentration was brought from zero to 28% by weight. The gel composition at 40% and 50% polyacrylamide was not homogeneous (the gel was not translucent). These results should therefore be considered with caution, since they reflect a different gel structure. Nonetheless, the data obtained seem consistent with the general trend. The crosslinker used (Bis or BAC) did not affect the measured relaxation times.

In order to maximize the homogeneity of the gel structure, BAC was preferred for the densest gels.[22] At concentrations of more than 40% polyacrylamide, however, all the samples became turbid after a few days. Note that the initial drop in T_1 is steeper than the decrease observed at higher fiber densities. This indicates that even fairly porous gels will hinder the tumbling of relatively small molecules considerably. It also reflects the fact that the effective pore size d_{av} does not decrease linearly with increasing gel concentration : as the gel gets denser, additional fibers have less effect.

A series of similar experiments was performed using agarose in concentrations up to 10%. The results reproduced in fig.5 show less dramatic changes in the relaxation time. This agrees with previous observations that the pores in agarose are larger than in polyacrylamide.

Measurements of transverse relaxation times T_2 were in qualitative agreement with the data for T_1. The apparent values of T_2 obtained in the Carr-Purcell-Meiboom-Gill spin-echo experiment,[23,24] however, were found to depend on the delay between refocusing pulses. This indicates a direct contribution of chemical exchange to the transverse relaxation time.[25] This additional dephasing mechanism made a direct comparison between T_1 and T_2 difficult, but the data seemed consistent if a systematic error of about 0.5 s due to chemical exchange was assumed. Either the observed scalar coupling between the phosphorus and a hydrogen atom on the sugar ring, or the coexistence of two conformations for the spin site, could give rise to this effect.

These experiments can be used to deduce valuable information about the gel structure. On the one hand, it is clear that the average pore size must be at least twice as large as the longest axis of a cGMP molecule, since no manifestation of extremely anisotropic motion was observed, even at the highest gel concentrations. Hence, as a rough estimate, one can evaluate $d_{av} > 16\,\mathring{A}$. An upper bound for the characteristic separation between the fibers is hard to deduce for this type of gel, since the translational diffusion of the molecule is rapid enough for the cGMP to pass

through many pores before the relaxation is complete. The near-encounters with polymer chains along its path account in part for the drop in rotational diffusion coefficient, in addition to the effect of the surrounding static matrix. It is interesting to note, however, that in a matrix with closed pores, each molecule would sample only one pore size ; it is then expected that relaxation measurements will provide very useful information not only about the average pore size, but also about the pore size distribution.

Since T_1 is proportional to kT/Ξ, the contribution of the fibers to the effective friction factor of the trapped molecule can be evaluated from $1/T_1$ - $1/T_1^{sol}$. Here, T_1^{sol} denotes the measured relaxation time in the absence of gel. A double logarithmic plot of this difference in relaxation rates versus gel concentration yields a slope very near unity for both polyacrylamide and agarose (fig.6). This indicates that the same mechanisms account for the slowing of the molecule, even though the gel structures are known to be very different. Agarose helices aggregate in bundles, leaving wide gaps between the fibers.[26,27] Polyacrylamide, on the other hand, forms a random network of polymer chains if the amount of crosslinking is less than five percent.[28] The experiments with agarose, where the pores are much wider than the molecular size of cGMP, suggest that the main interaction is due to the occasional encounters with the fibers, which couple the translational motion of the molecule to its rotation. More experimental data and a rigorous treatment of the hydrodynamics involved, however, will be needed to verify this conclusion.

3. Numerical Simulation

3.1 Fundamentals of Stokesian Dynamics

A more rigorous treatment of the hydrodynamics determining molecular diffusion in fibrous environments can be attempted by numerical simulation. This approach should aid in the interpretation of the experimental results, and will provide a theoretical background for cases which cannot adequately be described by macroscopic diffusion equations. The length scales involved in the process suggest that Stokesian dynamics[29] provides an adequate level of description. The small size of the solvent

molecules, as compared to the diffusing macromolecule, legitimates a continuum description of the solvent phase. The proteins, or other polymers of interest, can then be viewed as particles dispersed in a Newtonian fluid with the properties of water. The gel can be modeled as a network of solid rods, representing a single fiber or a bundle of polymer chains depending on the microstructure of the gel considered. Since the particle Reynolds number for the diffusing molecule is always much less than one, the inertial terms can be neglected in the Navier-Stokes equations for the solvent. The resulting quasi-stationary Stokes equation,

$$\nabla p = \mu \nabla^2 \mathbf{u} \tag{5}$$

balances pressure gradients ∇p in the fluid by viscous forces $\mu\nabla^2\mathbf{u}$. Of course, the solvent also satisfies the continuity equation, which takes the form $\nabla \cdot \mathbf{u} = 0$ for incompressible fluids. The motion of the N particles is described by a coupled N-body Langevin equation[30]

$$-\mathbf{m} \cdot \frac{d\mathbf{U}}{dt} = \mathbf{F}^H + \mathbf{F}^P + \mathbf{F}^B. \tag{6}$$

Here, $\mathbf{m}$ is a 6N $\times$ 6N generalized mass/moment of inertia matrix and $\mathbf{U}$ is the particle translational/rotational velocity vector of dimension 6N. Owing to the linearity of the Stokes equations, the hydrodynamic force $\mathbf{F}^H$ exerted by the particles is directly related to their relative velocity in the fluid and to the bulk shear stress $\mathbf{E}^\infty$ through resistance matrices which only depend on the instanteneous configuration of the system. In general,

$$\mathbf{F}^H = \mathbf{R}_{FU} \cdot (\mathbf{U} - \mathbf{U}^\infty) - \mathbf{R}_{FE} : \mathbf{E}^\infty. \tag{7}$$

The selfterms or diagonal elements of the resistance matrices $\mathbf{R}_{FU}$ and $\mathbf{R}_{FE}$ represent the drag on the particles. The off-diagonal coefficients (or crossterms) reflect viscous interactions between particles, and will bring into account the hydrodynamic effects of the static fibrous matrix on the Brownian particles. The vector $\mathbf{F}^P$ represents deterministic interparticle or external forces. Finally, the stochastic force $\mathbf{F}^B$ that gives rise to Brownian motion is characterized by

$$\langle \mathbf{F}^B \rangle = \mathbf{0} \qquad \text{and} \qquad \langle \mathbf{F}^B(0)\mathbf{F}^B(t) \rangle = 2\,kT\,\mathbf{R}_{FU}\,\delta(t). \tag{8}$$

Angular brackets denote an ensemble average. The magnitude of the autocorrelation function for the Brownian forces results from the fluctuation dissipation theorem and the equipartition principle for the thermal energy.

It should be noted that the validity of the Langevin equation rests on the assumption that all relaxation times associated with the fluids are short compared to those of the particles. This requires that the mass of the particles largely exceeds that of a solvent molecule.[31,32] Secondly, the configuration of the system should not change significantly during the time scale of Brownian motion[33] $\tau = m/6\pi\mu a$, which is the time required for the particle's momentum to relax after a Brownian impulse. Scaling arguments and rough estimates can be used to prove that this criterion is satisfied for typical particles ($1\,\mathrm{nm} < a < 1\,\mu\mathrm{m}$) in water at room temperature.[33] Finally, the vorticity of the fluid must diffuse faster than the particles lose inertia, i.e. $a^2/\nu << \tau$. This implies that the particles must be much denser than the fluid.[34] In cases where this condition is not satisfied, inertia must be taken explicitly into account. For a neutrally buoyant particle, the resulting velocity autocorrelation function $\mathbf{W}(t) = \langle \mathbf{U}(t_0)\mathbf{U}(t_0+t) \rangle$ decays as[35] $t^{-\frac{3}{2}}$ at times long compared to τ. This should be contrasted with the exponential behavior[34] obtained by integrating (6) with (7) and (8). In the course of a simulation, however, the particle will experience many uncorrelated Brownian impacts from the solvent molecules, and the long-time tail of the velocity autocorrelation function $\mathbf{W}(t)$ becomes irrelevant.[33] Indeed, at times larger than τ, only the low frequency components of the Fourier transform $\boldsymbol{\mathcal{W}}(\omega)$ of $\mathbf{W}(t)$ dominate the diffusion process because they provide the largest net displacements. Since these components represent almost steady motion, the *steady* hydrodynamic resistance functions $\mathbf{R}_{FU}$ and $\mathbf{R}_{FE}$ can be used in (7), and the omission of inertia is inconsequential.

Under these conditions, the Langevin equation can be integrated twice over a time step Δt chosen such that the configuration of the particles does not change much. The resulting displacements $\Delta\mathbf{x}$ in the 6N-dimensional position/orientation

space for the particles is given in non-dimensional form by[36]:

$$\Delta \mathbf{x} = Pe\{\mathbf{U}^{\infty} + (\mathbf{R}_{FU})^{-1} \cdot [\mathbf{R}_{FE} : \mathbf{E}^{\infty} - (\dot{\gamma}^*)^{-1}\mathbf{F}^P]\}\Delta t + \{\nabla \cdot (\mathbf{R}_{FU})^{-1}\Delta t + \mathbf{X}(\Delta t)\}. \tag{9}$$

Here, $\mathbf{x}$ has been non-dimensionalized by the characteristic particle size a. The time is set by the diffusive time scale a^2/D_0, where $D_0(= kT/6\pi\mu a)$ is the diffusion coefficient of an isolated spherical particle of radius a. The shear forces are scaled by $6\pi\mu a^2\dot{\gamma}$, with $\dot{\gamma} = |\mathbf{E}^{\infty}|$ the magnitude of the shear rate, and the interparticle forces by $|\mathbf{F}^P|$. The Péclet number $Pe = \dot{\gamma}a^2/D_0$ measures the relative importance of the shear and Brownian forces, and $\dot{\gamma}^* = 6\pi\mu a^2\dot{\gamma}/|\mathbf{F}^P|$ is a non-dimensional shear rate. For a Brownnian suspension, in the limit of $Pe \to 0$, the change $\Delta\mathbf{x}$ in the configuration of the particles consists of two terms : a random displacement $\mathbf{X}$, the stochastics of which are described by

$$\langle \mathbf{X} \rangle = \mathbf{0} \qquad \text{and} \qquad \langle \mathbf{X}(\Delta t)\, \mathbf{X}(\Delta t) \rangle = 2(\mathbf{R}_{FU})^{-1}\Delta t, \tag{10}$$

and a displacement due to the configuration space divergence of the N-particle mobility matrix, $\nabla \cdot (\mathbf{R}_{FU})^{-1}\Delta t$.

Obviously, the mobility tensor $\mathbf{M} = \mathbf{R}_{FU}^{-1}$ plays a central role in the dynamics of the particulate system. Due to the complexity of many-body hydrodynamic interactions, a pairwise additivity scheme must be adopted in constructing an approximation for $\mathbf{M}$. The velocity disturbance of one body caused by an external force applied to another, "senses" third body effects at $O(r^{-4})$, where r is a characteristic particle separation.[37] In the resistance matrix, however, the presence of the third particle appears at $O(r^{-2})$.[33] Thus it seems that pairwise additivity of velocities (the so-called mobility formulation) is more accurate than the resistance formulation for systems of widely spaced particles. However, lubrication forces will only be preserved by including them directly in the resistance matrix. Durlofsky et al. therefore proposed an algorithm which combines both methods.[38] It yields a resistance matrix which accurately represents the lubrication forces, and which even includes some many-body resistance interactions. This is accomplished by inverting

the N-body mobility matrix constructed by assuming a pairwise additivity of velocities. Lubrication effects are then added directly to this far-field approximation of the resistance matrix, using the exact two-body resistance functions[39]. Since some two-body interactions were already included in the invert of the mobility tensor, a corrective step ensures that these contributions are not counted twice. This formalism yields an accurate approximation for the N-body resistance matrix at all particle separations.

3.2 Prediction of Diffusivities from Stokesian Dynamics

The generalized Stokes-Einstein equation relates the diffusion tensor of an arbitrary body to its hydrodynamic resistance tensor. As shown by Brenner,[14] $\mathbf{D} = kT\mathbf{R}_{FU}^{-1} = kT\mathbf{M}$. The short-time self-diffusivity $\mathbf{D}_0^s$ is found by taking the trace over all particles of the selfterms in the diffusion tensor, and averaging over all configurations :

$$\mathbf{D}_0^s = \langle tr_p\, \mathbf{D} \rangle = kT \langle tr_p\, \mathbf{R}_{FU}^{-1} \rangle. \tag{11}$$

It measures the body's instanteneous mobility. The long time self-diffusivity $\mathbf{D}_\infty^s$, on the other hand, characterizes a particle's tendency to wander far from its initial position in configuration space and is given by[30]:

$$\mathbf{D}_\infty^s = \lim_{t\to\infty} \frac{1}{2}\frac{d}{dt}\Big\langle tr_p\big(\mathbf{x} - \langle \mathbf{x} \rangle\big)\big(\mathbf{x} - \langle \mathbf{x} \rangle\big)\Big\rangle. \tag{12}$$

A Stokesian dynamics simulation of molecular diffusion in fibrous media complements the experimental nuclear magnetic relaxation studies very nicely since the orientational autocorrelation function $\langle Y_2^{-m}(\Omega(0)) Y_2^m(\Omega(t)) \rangle$ which determines the spectral density $J_2^m(\omega)$ in (3), follows in a straightforward fashion from the calculated particle trajectories in configuration space. In order to focus on the influence of the gel matrix on molecular diffusion, infinitely dilute suspensions can be considered. In this limit, one follows the path of a single test particle caught in a network of stiff rods with which it interacts hydrodynamically. The fibers being fixed in space, the Langevin equation only needs to be solved for the six components of the particle's velocity, even though the full N-body mobility matrix needs to be inverted

to preserve many-body effects. Since only N of the N(N-1) interactions between particles evolve in time, these simulations should be much less computer intensive than the numerical solution of many other many-body problems.

3.3 Hydrodynamic Interactions between Prolate Spheroids in the Mobility Formulation

Considering the central role played by the resistance tensor $\mathbf{R}_{FU}$ in the evolution of the system, it is mandatory to reproduce hydrodynamic interactions as accurately as possible. Even though remarkably good agreement with slender body theory has been obtained in a previous series of Stokesian dynamics experiments[38] by approximating prolate spheroids as a string of touching spheres, a more direct approach must incorporate hydrodynamic interactions between spheroids directly. By considering each particle as an entity, rather than a composite body, the accuracy of the method should improve significantly. The accompanying reduction in the number of degrees of freedom should also markedly increase the efficiency of the numerical simulations. Clearly, a gel matrix is also more satisfactorily, and more economically, modeled as a network of long, slender rods than as chains of closely spaced spheres. Similarly, the ellipsoidal shape of many biopolymers, such as chymotrypsin[2] and lysozyme,[40] will be closely fitted by a prolate spheroid.

Following the algorithm proposed by Durlofsky et al.,[38] the first step in the construction of the resistance matrix is the inversion of a mobility tensor obtained by pairwise additivity of velocities. Hence the extension of Stokesian dynamics to suspensions of prolate spheroids requires a knowledge of the mobility interactions between such bodies.

The velocity disturbance caused by a prolate spheroid in a uniform stream $\mathbf{U}^\infty$, a constant vorticity field $\mathbf{\Omega}^\infty$ and a rate-of-strain field $\mathbf{E}^\infty$ can be generated by an equivalent distribution of singularities along the line joining the foci of the ellipsoid.[41,42] The velocity at any point in the fluid can therefore be evaluated by a line integral (see appendix A). A theorem due to Kim[43], which is essentially an extension of the reciprocal theorem of Lorentz[44], then predicts that the Faxèn laws

for the force, torque and stresslet exerted by a prolate spheroid in an arbitrary ambient flow $\mathbf{u}^\infty$ can be written as line integrals of $\mathbf{u}^\infty$ over the particle axis[43] (appendix A). By combining these expressions with the results of Chwang and Wu,[41,42] the velocity disturbance in the applied flow due to the presence of a prolate spheroid, can be related to the generalized force ($\mathbf{F}$, $\mathbf{T}$, $\mathbf{S}$) experienced by the fluid. Secondly, the Faxèn laws derived by Kim[43] can be inverted to yield the imposed linear shear field $\mathbf{E}^\infty$ and the relative velocity ($\mathbf{U} - \mathbf{U}^\infty$, $\boldsymbol{\omega} - \boldsymbol{\Omega}^\infty$) of the particle in terms of its generalized force and the local deviations $\mathbf{u}'^\infty$ from the applied flow (appendix A). In the case of non-spherical objects, this operation is complicated by the coupling of the angular velocity $\boldsymbol{\omega}$ to the rate of strain $\mathbf{E}^\infty$.

By realizing that the ambient flow experienced by a given body is simply the velocity disturbance due to the presence of all other particles, the hydrodynamic interactions between pairs of prolate spheroids can now be determined in the mobility formulation (appendix A). The resulting mobility tensor can be shown to satisfy all the symmetry requirements set by the reciprocal theorem of Lorentz.[44] Although it is usually applied to the selfterms of the mobility matrix,[45,46] the reciprocal theorem also predicts useful relations between crossterms (see appendix D).

3.4 Numerical Aspects

In constructing the mobility matrix for a given configuration of the particulate system, a double integration over the particle axes must be carried out for each pair of interacting spheroids. The orientations $\mathbf{d}_1$ and $\mathbf{d}_2$ of the ellipsoids, and their separation, is arbitrary. Using cylindrical coordinates centered at the origin of spheroid "2" with the azimuthal axis along $\mathbf{d}_2$ (fig.7), the first integration in (A.18) can be carried out analytically. The result is most conveniently expressed in terms of the coefficients $B_{m,n}(\mathbf{x})$ introduced by Chwang and Wu[42] as

$$B_{m,n}(\mathbf{x}) = \int_{-c_2}^{c_2} \frac{\xi^n}{|\mathbf{x} - \boldsymbol{\xi}|^m}\, d\xi. \tag{13}$$

A recurrence relation for $B_{m,n}(\mathbf{x})$ makes this formulation especially suited for com-

puter programming. It is easily shown using integration by parts that

$$B_{m,n}(\mathbf{x}) = -\frac{c_2^{n-1}}{m-2}\left(\frac{1}{R_2^{m-2}} + \frac{(-1)^n}{R_1^{m-2}}\right) + \frac{n-1}{m-2}B_{m-2,n-2} + xB_{m,n-1} \qquad (14)$$

for n ≥ 2, where x, R_1 and R_2 are defined in fig.7.

Taking advantage of identities relating the derivatives of $B_{m,n}(\mathbf{x})$ (appendix B), and after a formidable amount of tedious but straightforward algebra, all the mobility coefficients involving particles "1" and "2" can be written in the form

$$\frac{1}{\mu}\int_{-c_1}^{c_1} f\left(\{B_{m,n}(\xi_1)\}; c_1, c_2, e_1, e_2\right) d\xi_1 \qquad (15)$$

where $f\left(\{B_{m,n}\}\right)$ is a linear function of the set of $B_{m,n}(\mathbf{x})$. Twenty-four different combinations of m and n appear in the expressions for $f\left(\{B_{m,n}\}\right)$. The index m can take on any odd integer value between 1 and 9, and n varies from 0 to $\min\{5, m\}$. All these coefficients are known in closed form. However, at large separations ($x/c_2 > 6$ or $r/c_2 > 8$), the analytical formulae become numerically unstable. (They involve the difference between the endpoint-values of the integral, which becomes increasingly small as the distance between the foci, $2c_2$, decreases relative to $(x^2+r^2)^{\frac{1}{2}}$.) Fortunately, the $B_{m,n}(\mathbf{x})$ can accurately be calculated by numerical integration techniques, and Simpson's method was found to converge rapidly when $(x^2+r^2)^{\frac{1}{2}} >> c_2$. A more serious drawback of the exact expressions for $B_{m,n}(\mathbf{x})$ is their inadequate form when $r \to 0$. Indeed, for $m \neq 1$,

$$B_{m,0}(\mathbf{x}) = \frac{1}{r^{m-1}}\sum_{k=0}^{(m-3)/2}\frac{(-1)^k}{2k+1}\binom{(m-3)/2}{k}\left\{\frac{(x+c_2)^{2k+1}}{R_1^{2k+1}} - \frac{(x-c_2)^{2k+1}}{R_2^{2k+1}}\right\} \qquad (16)$$

For $r/c_2 < 10^{-2}$, a Taylor series expansion about $r = 0$ is used to overcome this problem. The series is truncated so that the mobility coefficients would be accurate to $O\left((r/c_2)^6\right)$ at least.

Once the $B_{m,n}(\xi_1)$ are known, the function $f\left(\{B_{m,n}\}\right)$ in (15) is integrated numerically. At each point along the discretization axis, this requires converting the local cylindrical coordinate system used for the first integration (at fixed ξ_1),

back to the cartesian "laboratory frame of reference". A flowchart for constructing the crossterms in the mobility matrix is given in fig.8 .

At this point, the theory of pairwise interactions between prolate spheroids in low Reynolds number linear flows is complete at the level of forces, torques and stresslets. The invert of this approximate mobility matrix yields a far-field estimate of the resistance tensor. Note also that the formulae allow for a distribution of aspect ratios, since it is never assumed in the discussion above that the interacting particles have the same eccentricity e. In particular, mobility interactions between spheres ($e \rightarrow 0$), rods ($e \rightarrow 1$) and other prolate spheroids are adequately represented by equations like (A.18). Due to computational limitations, the range of aspect ratios acceptable in the current version of the code is large, but finite. A glance at the expressions in Appendix C will indicate some of the difficulties encountered in both limits $e \rightarrow 0$ and $e \rightarrow 1$.

4. Conclusions

Considerable progress has been made towards the extension of Stokesian dynamics to prolate spheroids. The mobility matrix can be constructed exactly at the level of forces, torques and stresslets. This represents an important step towards the development of a new version of Stokesian dynamics specific for suspensions of prolate spheroids, which will allow computer-efficient numerical simulations of molecular diffusion in fibrous environments to be performed.

The application of nuclear magnetic relaxation measurements to study rotational motions in opaque gels looks promising. The type of motions that can be monitored spans an impressive range, covering rapid tumbling in non-viscous fluids, with characteristic correlation times of the order of picoseconds, as well as much slower, hindered motions that can occur in porous media. The spectrum of frequencies to which the technique is sensitive can be enlarged even further by observing different nuclei (any spin other than hydrogen will do), by varying the magnetic field, or by a clever selection of the experiments : the transverse relaxation time T_2 and the spin-lattice relaxation in the rotating frame for example, reveal the low

frequency components of the motions. Finally, the dependence of NMR on both the rate and the geometry of the molecular tumbling make relaxation measurements a very powerful and attractive tool to study matrix-induced anisotropic diffusion.

APPENDIX A

Outline of the Calculation of Hydrodynamic Interactions between Prolate Spheroids in the Mobility Formulation

Starting from the fundamental solution of the Stokes equations, Chwang & Wu[41,42] constructed exact solutions for several low Reynolds number problems involving rigid boundaries. In particular, they showed that the velocity disturbance caused by a prolate spheroid in a uniform stream $\mathbf{U}^\infty$, a constant vorticity field $\mathbf{\Omega}^\infty$ and a rate-of-strain field $\mathbf{E}^\infty$, is reproduced by a uniform, parabolic, or biquadratic distribution of singularities along the particle's major axis. The velocity $\mathbf{u}(\mathbf{x})$ at any point in the fluid can then be evaluated by a line integral[43]:

$$\begin{aligned}\mathbf{u}(\mathbf{x}) =&\mathbf{U}^\infty - \mathbf{U}^\infty \cdot \{\alpha_1 \mathbf{dd} + \alpha_2(\boldsymbol{\delta} - \mathbf{dd})\} \cdot \\ &\cdot \int_{-c}^{c} \left\{1 + (c^2 - \xi^2)\frac{(1-e^2)}{4e^2}\nabla^2\right\}\mathbf{I}(\mathbf{x}-\boldsymbol{\xi})\, d\xi, \qquad (A.1)\end{aligned}$$

$$\begin{aligned}\mathbf{u}(\mathbf{x}) =&\mathbf{\Omega}^\infty \wedge \mathbf{x} + \frac{1}{2}\mathbf{\Omega}^\infty \cdot \{\gamma \mathbf{dd} + \gamma'(\boldsymbol{\delta} - \mathbf{dd})\} \cdot \int_{-c}^{c} (c^2 - \xi^2)\nabla \wedge \mathbf{I}(\mathbf{x}-\boldsymbol{\xi})\, d\xi + \\ &+ \alpha_1 \int_{-c}^{c} (c^2 - \xi^2)\left\{1 + (c^2 - \xi^2)\frac{(1-e^2)}{8e^2}\nabla^2\right\} \mathbf{K}(\mathbf{x}-\boldsymbol{\xi}) : (\mathbf{\Omega}^\infty \wedge \mathbf{d})\mathbf{d}\, d\xi, \qquad (A.2)\end{aligned}$$

and

$$\begin{aligned}u_i(\mathbf{x}) =&E_{ij}x_j - E_{lm}\left\{\frac{\alpha_5}{2}\left(d_j d_k - \frac{1}{3}\delta_{jk}\right)\left(d_l d_m - \frac{1}{3}\delta_{lm}\right)\right. \\ &+ \frac{\alpha^*}{4}(d_j\delta_{km}d_l + d_j\delta_{kl}d_m + \delta_{jm}d_k d_l + \delta_{jl}d_k d_m - 4d_j d_k d_l d_m) \\ &+ \frac{\alpha_4}{2}(\delta_{jl}\delta_{km} + \delta_{jm}\delta_{kl} - \delta_{jk}\delta_{lm} + d_j d_k \delta_{lm} + \delta_{jk}d_l d_m \qquad (A.3) \\ &\left. - d_j\delta_{km}d_l - \delta_{jm}d_k d_l - d_j\delta_{kl}d_m - \delta_{jl}d_k d_m + d_j d_k d_l d_m)\right\}\cdot \\ &\cdot \int_{-c}^{c} (c^2 - \xi^2)\left\{1 + (c^2 - \xi^2)\frac{(1-e^2)}{8e^2}\nabla^2\right\} I_{ij,k}(\mathbf{x}-\boldsymbol{\xi})\, d\xi \\ &- E_{lm}d_j\delta_{km}d_l\alpha_1 \int_{-c}^{c} (c^2 - \xi^2)\frac{1}{2}\left\{I_{ij,k}(\mathbf{x}-\boldsymbol{\xi}) - I_{ik,j}(\mathbf{x}-\boldsymbol{\xi})\right\} d\xi.\end{aligned}$$

Here, $\mathbf{d}$ is the unit vector along the spheroidal axis, and $\mathbf{I}$ is the Oseen tensor,

$$\mathbf{I}(\mathbf{x}) = \frac{\boldsymbol{\delta}}{|\mathbf{x}|} + \frac{\mathbf{xx}}{|\mathbf{x}|^3}. \qquad (A.4)$$

$I_{ij,k} = (\nabla \mathbf{I})_{kij}$ and $K_{ijk} = \frac{1}{2}(I_{ij,k} + I_{ik,j})$. All the remaining parameters depend only on the geometry of the prolate body : c is the center-to-focus distance and $e = c/a$, where $2a$ is the length of the major axis. The quantities α and γ are functions of e, given in appendix C. In a short and elegant proof, Kim shows that the Faxèn law for the force $\mathbf{F}$ on an immobile slip-free rigid particle in an arbitrary ambient velocity field $\mathbf{u}^\infty$ has the same functional form as the singularity solution for the velocity disturbance $\mathbf{u}'$ in a uniform stream $\mathbf{U}^\infty$ past the same stationary body[43]:

$$\text{if} \qquad \mathbf{u}'(\mathbf{x}) = \mathbf{u}(\mathbf{x}) - \mathbf{U}^\infty = \mathbf{U}^\infty \cdot \frac{L_\xi\Big\{\mathbf{I}(\mathbf{x}-\xi)\Big\}}{8\pi\mu} \tag{A.5}$$

where L_ξ is a linear functional, then

$$\mathbf{F} = -L_\xi\Big\{\mathbf{u}^\infty(\xi)\Big\}. \tag{A.6}$$

Here ξ denotes the distribution of singularities. Based on this theorem and the results of Chwang and Wu,[41,42] Kim derives the Faxèn laws for a prolate spheroid moving at $\mathbf{U} + \boldsymbol{\omega} \wedge \mathbf{x}$ ($\mathbf{x}$ measured from the geometrical center of the particle). The force $\mathbf{F}$, the torque $\mathbf{T}$ and the stresslet $\mathbf{S}$ exerted by the body on the fluid can be written as†

$$\begin{aligned}\mathbf{F} =& 16\pi\mu c\{\alpha_1 \mathbf{dd} + \alpha_2(\boldsymbol{\delta} - \mathbf{dd})\} \cdot \mathbf{U} \\ &- 8\pi\mu\{\alpha_1 \mathbf{dd} + \alpha_2(\boldsymbol{\delta} - \mathbf{dd})\} \cdot \int_{-c}^{c} \Big\{1 + (c^2 - \xi^2)\frac{(1-e^2)}{4e^2}\nabla^2\Big\}\mathbf{u}^\infty(\xi)\, d\xi,\end{aligned} \tag{A.7}$$

$$\begin{aligned}\mathbf{T} =& \frac{32}{3}\pi\mu c^3\{\gamma \mathbf{dd} + \gamma'(\boldsymbol{\delta} - \mathbf{dd})\} \cdot \boldsymbol{\omega} \\ &- 4\pi\mu\{\gamma \mathbf{dd} + \gamma'(\boldsymbol{\delta} - \mathbf{dd})\} \cdot \int_{-c}^{c} (c^2 - \xi^2)\nabla \wedge \mathbf{u}^\infty(\xi)\, d\xi \\ &- 8\pi\mu\alpha_1 \mathbf{d} \wedge \int_{-c}^{c} (c^2 - \xi^2)\Big\{1 + (c^2 - \xi^2)\frac{(1-e^2)}{8e^2}\nabla^2\Big\}\mathbf{d} \cdot \mathbf{e}^\infty(\xi)\, d\xi\end{aligned} \tag{A.8}$$

† In the special case of one spheroid moving at a velocity ($\mathbf{U}$, $\boldsymbol{\omega}$) in a stream characterized by $\mathbf{U}^\infty$, $\boldsymbol{\Omega}^\infty$ and $\mathbf{E}^\infty$, these expressions can be shown to include the results obtained previously by Brenner.[47] The comparison is quite laborious due to a different choice of variables and a different grouping of the tensor components in both papers.

and

$$
\begin{aligned}
S_{ij} =& 8\pi\mu\Big\{\frac{\alpha_5}{2}\Big(d_id_j-\frac{1}{3}\delta_{ij}\Big)\Big(d_kd_l-\frac{1}{3}\delta_{kl}\Big)\\
&+\frac{\alpha^*}{4}(d_i\delta_{jk}d_l+d_i\delta_{jl}d_k+\delta_{il}d_jd_k+\delta_{ik}d_jd_l-4d_id_jd_kd_l)\\
&+\frac{\alpha_4}{2}(\delta_{ik}\delta_{jl}+\delta_{il}\delta_{jk}-\delta_{ij}\delta_{kl}+d_id_j\delta_{kl}+\delta_{ij}d_kd_l \qquad \text{(A.9)}\\
&-d_i\delta_{jl}d_k-\delta_{ik}d_jd_l-d_i\delta_{jk}d_l-\delta_{il}d_jd_k+d_id_jd_kd_l)\Big\}\cdot\\
&\cdot\int_{-c}^{c}(c^2-\xi^2)\Big\{1+(c^2-\xi^2)\frac{(1-e^2)}{8e^2}\nabla^2\Big\}e^{\infty}_{kl}(\boldsymbol{\xi})\,d\xi\\
&-2\pi\mu\alpha_1(d_i\epsilon_{jkl}d_l+d_j\epsilon_{ikl}d_l)\int_{-c}^{c}(c^2-\xi^2)\big\{\nabla\wedge\mathbf{u}^{\infty}(\boldsymbol{\xi})-2\boldsymbol{\omega}\big\}_k\,d\xi.
\end{aligned}
$$

These integral expressions are easier to handle in numerical simulations than the infinite series of operators obtained by Brenner,[45] who expanded the ambient field in a Taylor series at the particle center.

The mobility functions can be obtained by inverting the Faxèn laws (A.7)-(A.9). It is readily found that :

$$
\begin{aligned}
\mathbf{U}-\mathbf{U}^{\infty} =& \frac{1}{16\pi\mu c}\{\alpha_1^{-1}\mathbf{dd}+\alpha_2^{-1}(\boldsymbol{\delta}-\mathbf{dd})\}\cdot\mathbf{F}\\
&+\frac{1}{2c}\int_{-c}^{c}\Big\{1+(c^2-\xi^2)\frac{(1-e^2)}{4e^2}\nabla^2\Big\}\mathbf{u}'^{\infty}(\boldsymbol{\xi})\,d\xi, \qquad \text{(A.10)}
\end{aligned}
$$

but the expressions for $\boldsymbol{\omega}$ and $\mathbf{E}^{\infty}$ are coupled. In a uniform purely straining flow $\mathbf{E}^{\infty}=\frac{1}{2}(\nabla\mathbf{u}^{\infty}+(\nabla\mathbf{u}^{\infty})^T)=\nabla\mathbf{u}^{\infty}$, the two contributions to the stresslet reflect this coupling : one term arises directly from the rate-of-strain field, the other is due to the induced rotation of the particle. The result can be cast in the general form

$$
\mathbf{S}=\mathbf{R}'_{SE}:\mathbf{E}^{\infty}+\mathbf{R}'_{S\omega}\cdot\boldsymbol{\omega}. \qquad \text{(A.11)}
$$

Equation (A.8) is easily rearranged to give $\boldsymbol{\omega}$ as a function of $\mathbf{T}$, $\nabla\wedge\mathbf{u}^{\infty}$ and $\mathbf{e}^{\infty}$. For a torque-free spheroid in a flow of constant vorticity $\boldsymbol{\Omega}^{\infty}$ and uniform rate of

strain $\mathbf{E}^\infty$, the expression reduces to †

$$\boldsymbol{\omega} = \boldsymbol{\Omega}^\infty + \frac{e^2}{2-e^2}\mathbf{d}\wedge\mathbf{d}\cdot\mathbf{E}^\infty. \tag{A.12}$$

Inserting this relation, with $\boldsymbol{\Omega}^\infty = 0$ in (A.11), a linear relation between the stresslet and the rate of strain can be derived for a torque-free prolate spheroid in a uniform irrotational straining flow :

$$\mathbf{S} = (\mathbf{R}'_{SE} + \frac{e^2}{2-e^2}\mathbf{R}'_{S\omega}\wedge\mathbf{dd}) : \mathbf{E}^\infty = \mathbf{R}_{SE} : \mathbf{E}^\infty. \tag{A.13}$$

By exploiting the symmetry of $\mathbf{E}^\infty$ and expanding $\mathbf{R}_{SE}$ in a set of orthogonal fourth order tensors, the inverse relation was obtained in explicit form, i.e. $\mathbf{E}^\infty = \mathbf{M}_{ES} : \mathbf{S}$. The elimination of $\boldsymbol{\omega}$ from (A.8) and (A.9), yields $\mathbf{S}$ as a function of $\mathbf{e}^\infty$ and $\mathbf{T}$. It is interesting to note that two terms involving $\nabla\wedge\mathbf{u}^\infty$ cancel each other during this manipulation. Limiting our discussion to imposed linear flow fields, ‡ it is then possible to separate $\mathbf{e}^\infty$ into a uniform applied shear field $\mathbf{E}^\infty$ and a disturbance on the main straining flow $\mathbf{e}'^\infty$. A double-dot left-multiplication by $\mathbf{M}_{ES}$ on both sides of the equation, followed by some simplifications, then yields a mobility expression for the ambient rate of strain $\mathbf{E}^\infty$ in terms of $\mathbf{S}$, $\mathbf{T}$ and $\mathbf{e}'^\infty$. Plugging this expression into (A.8) to eliminate $\mathbf{E}^\infty$, we obtain the following Faxèn formulae for the mobility

---

† An equivalent formulation, in terms of the aspect ratio r_p of the particle, reads :

$$\dot{\mathbf{d}} = \boldsymbol{\omega}\wedge\mathbf{d} + \frac{r_p^2-1}{r_p^2+1}(\mathbf{d}\cdot\mathbf{E}^\infty - \mathbf{d}\cdot\mathbf{E}^\infty\cdot\mathbf{dd})$$

‡ It is not meaningful to consider imposed quadratic velocity fields because the boundaries creating such flows contribute to the motion of the particle to the same order as the curvature of the flow.[38]

of prolate spheroids :

$$\begin{aligned}\boldsymbol{\omega}-\boldsymbol{\Omega}^{\infty} =& \frac{3}{32\pi\mu c^3}\left\{\gamma^{-1}\mathbf{dd}+\gamma'^{-1}(\boldsymbol{\delta}-\mathbf{dd})+\frac{e^2/(2-e^2)}{\left(\frac{2-e^2}{e^2}\alpha^*+\alpha_1\right)}(\mathbf{dd}-\boldsymbol{\delta})\right\}\cdot\mathbf{T}\\ &-\frac{3}{32\pi\mu c^3}\frac{1}{\left(\frac{2-e^2}{e^2}\alpha^*+\alpha_1\right)}(\mathbf{d}\wedge\mathbf{S}\cdot\mathbf{d}-\mathbf{d}\cdot\mathbf{S}\wedge\mathbf{d}) \qquad \text{(A.14)}\\ &+\frac{3}{8c^3}\int_{-c}^{c}(c^2-\xi^2)\nabla\wedge\mathbf{u}'^{\infty}(\boldsymbol{\xi})\,d\xi\end{aligned}$$

and

$$\begin{aligned}-E_{ij}^{\infty} =& \frac{3}{32\pi\mu c^3}\left\{\frac{9}{2\alpha_5}\left(d_id_j-\frac{1}{3}\delta_{ij}\right)\left(d_kd_l-\frac{1}{3}\delta_{kl}\right)\right.\\ &+\frac{1}{\left(\alpha^*+\frac{e^2}{2-e^2}\alpha_1\right)}(d_i\delta_{jk}d_l+d_i\delta_{jl}d_k+\delta_{il}d_jd_k+\delta_{ik}d_jd_l-4d_id_jd_kd_l)\\ &+\frac{1}{2\alpha_4}(\delta_{ik}\delta_{jl}+\delta_{il}\delta_{jk}-\delta_{ij}\delta_{kl}+d_id_j\delta_{kl}+\delta_{ij}d_kd_l \qquad \text{(A.15)}\\ &\left.-d_i\delta_{jl}d_k-\delta_{ik}d_jd_l-d_i\delta_{jk}d_l-\delta_{il}d_jd_k+d_id_jd_kd_l)\right\}S_{kl}\\ &+\frac{3}{4c^3}\int_{-c}^{c}(c^2-\xi^2)\left\{1+(c^2-\xi^2)\frac{(1-e^2)}{8e^2}\nabla^2\right\}e_{ij}'^{\infty}(\boldsymbol{\xi})\,d\xi\\ &-\frac{3}{32\pi\mu c^3}\frac{1}{\left(\frac{2-e^2}{e^2}\alpha^*+\alpha_1\right)}(\mathbf{dd}\wedge\mathbf{T}-\mathbf{T}\wedge\mathbf{dd})_{ij}\end{aligned}$$

These relations determine the motion of a particle immersed in a flow field given by $\mathbf{U}^{\infty}+\boldsymbol{\omega}^{\infty}\wedge\mathbf{x}+\mathbf{e}^{\infty}\cdot\mathbf{x}+\mathbf{u}'^{\infty}(\mathbf{x})$. Note that $\mathbf{e}'^{\infty}=\frac{1}{2}\left(\nabla\mathbf{u}'+(\nabla\mathbf{u}')^T\right)$. The mobility representation of the hydrodynamic interactions will be complete when the disturbance velocity field $\mathbf{u}'^{\infty}$ caused by all other particles is expressed as a function of the generalized force ($\mathbf{F}$, $\mathbf{T}$, $\mathbf{S}$) exerted by these bodies. From the linearity of the creeping flow equations, it follows that the velocity at any point in the fluid is a linear superposition of the contributions of $\mathbf{F}$, $\mathbf{T}$ and $\mathbf{S}$ exerted by each particle separately. By combining (A.1)-(A.3) and (A.7)-(A.9), the velocity disturbance caused by a particle exerting a force $\mathbf{F}$, a torque $\mathbf{T}$ and a stresslet $\mathbf{S}$

on the fluid is found to be :

$$\begin{aligned}\mathbf{u}'(\mathbf{x}) =& \frac{1}{16\pi\mu c}\mathbf{F}\cdot\int_{-c}^{c}\{1+(c^2-\xi^2)\frac{(1-e^2)}{4e^2}\nabla^2\}\mathbf{I}(\mathbf{x}-\boldsymbol{\xi})\,d\xi \\ &- \frac{3}{64\pi\mu c^3}\mathbf{T}\cdot\int_{-c}^{c}(c^2-\xi^2)\nabla\wedge\mathbf{I}(\mathbf{x}-\boldsymbol{\xi})\,d\xi \qquad \text{(A.16)} \\ &+ \frac{3}{32\pi\mu c^3}\int_{-c}^{c}(c^2-\xi^2)\{1+(c^2-\xi^2)\frac{(1-e^2)}{8e^2}\nabla^2\}\mathbf{K}(\mathbf{x}-\boldsymbol{\xi})\,d\xi \quad :\mathbf{S}.\end{aligned}$$

In the limit of $e \to 0$ at finite a, the irreducible moments expansion for the velocity disturbance created by a sphere immersed in a linear flow field can be recovered :

$$\begin{aligned}\mathbf{u}'(\mathbf{x}) =& \frac{1}{8\pi\mu}\{(1+\frac{a^2}{6}\nabla^2)\mathbf{I}(\mathbf{x})\cdot\mathbf{F}+\mathbf{R}(\mathbf{x})\cdot\mathbf{T} \\ &+(1+\frac{a^2}{10}\nabla^2)\mathbf{K}(\mathbf{x}):\mathbf{S}\} \qquad \text{(A.17)}\end{aligned}$$

where[38] $\mathbf{R}(\mathbf{x}) = \frac{1}{2}(\nabla\wedge\mathbf{I}(\mathbf{x}))^T$. By summing (A.16) over all particles interacting with particle "1", inserting the result into the mobility functions (A.10),(A.14) and (A.15) of spheroid "1", and repeating this for all particles, the mobility matrix for a system of N prolate spheroids can be constructed at the level of forces, torques and stresslets. For example, the contribution of a force $\mathbf{F}_2$ on particle "2" to the translational velocity $\mathbf{U}_1$ of a first body is given by :

$$\begin{aligned}\mathbf{U}_1 =& \frac{1}{32\pi\mu c_1 c_2}\int_{-c_1}^{c_1}\Big[\{1+(c_1^2-\xi_1^2)\frac{(1-e_1^2)}{4e_1^2}\nabla^2\} \qquad \text{(A.18)} \\ &\int_{-c_2}^{c_2}\{1+(c_2^2-\xi_2^2)\frac{(1-e_2^2)}{4e_2^2}\nabla^2\}\mathbf{I}(\boldsymbol{\xi}_1-\boldsymbol{\xi}_2)\Big]\,d\xi_2\,d\xi_1\cdot\mathbf{F}_2\end{aligned}$$

The resulting mobility tensor can then be inverted to yield a far-field approximation of the resistance tensor.

APPENDIX B

Chwang & Wu's $B_{m,n}(\mathbf{x})$coefficients

The coefficients $B_{m,n}(\mathbf{x})$ are defined as (see also fig.7)

$$B_{m,n}(\mathbf{x}) = \int_{-c_2}^{c_2} \frac{\xi^n}{|\mathbf{x}-\boldsymbol{\xi}|^m}\, d\xi \tag{B.1}$$

with $n = 0, 1, 2, \ldots$ and $m = 1, 3, 5, \ldots$

Defining

$$R_1(\mathbf{x}) = \{(x+c_2)^2 + r^2\}^{\frac{1}{2}} \qquad \text{and} \qquad R_2(\mathbf{x}) = \{(x-c_2)^2 + r^2\}^{\frac{1}{2}}, \tag{B.2}$$

the recurrence formula (14) can be proved by integrating $B_{m,n}(\mathbf{x})$ by parts. The initial values $B_{m,0}(\mathbf{x})$ are given by (16) for $m \neq 0$ and by

$$B_{1,0}(\mathbf{x}) = \log \frac{R_2 - (x-c)}{R_1 - (x+c)} = \log \frac{R_1 + (x+c)}{R_2 + (x-c)} \tag{B.3}$$

if $m = 0$. The recurrence formula (14) also applies for $n = 1$ if the second term is set to zero. For example,

$$B_{1,1}(\mathbf{x}) = R_2 - R_1 + xB_{1,0}(\mathbf{x}). \tag{B.4}$$

Some useful identities involving the derivatives of $B_{m,n}(\mathbf{x})$ are :

$$r\frac{\partial}{\partial x}B_{m,n} = \frac{\partial}{\partial r}(xB_{m,n} - B_{m,n+1}) \tag{B.5}$$

$$x\frac{\partial}{\partial x}B_{m,n} - \frac{\partial}{\partial x}B_{m,n+1} + r\frac{\partial}{\partial r}B_{m,n} = -mB_{m,n} \tag{B.5}$$

$$\nabla^2 B_{m,n} = \frac{\partial^2}{\partial x^2}B_{m,n} + \frac{\partial^2}{\partial r^2}B_{m,n} + \frac{1}{r}\frac{\partial}{\partial r}B_{m,n} = m(m-1)B_{m+2,n} \tag{B.6}$$

$$\frac{\partial^2}{\partial x^2}B_{m,n} + \frac{\partial^2}{\partial r^2}B_{m,n} + \frac{m}{r}\frac{\partial}{\partial r}B_{m,n} = 0 \tag{B.7}$$

APPENDIX C

Functions α and γ

Following the notation of Kim[43]

$$\alpha_1 = e^2 \left\{ -2e + (1+e^2) \log\left(\frac{1+e}{1-e}\right) \right\}^{-1} \tag{C.1}$$

$$\alpha_2 = 2e^2 \left\{ 2e + (3e^2-1) \log\left(\frac{1+e}{1-e}\right) \right\}^{-1} \tag{C.2}$$

$$\gamma = (1-e^2) \left\{ 2e + (1-e^2) \log\left(\frac{1+e}{1-e}\right) \right\}^{-1} \tag{C.3}$$

$$\gamma' = (2-e^2) \left\{ -2e + (1+e^2) \log\left(\frac{1+e}{1-e}\right) \right\}^{-1} \tag{C.4}$$

$$\gamma_3' = \left\{ -2e + (1+e^2) \log\left(\frac{1+e}{1-e}\right) \right\}^{-1} \tag{C.5}$$

$$\alpha^* = e^2 \gamma_3' \left\{ 2e(2e^2-1) + (1-e^2) \log\left(\frac{1+e}{1-e}\right) \right\} \cdot \left\{ 2e(2e^2-3) + 3(1-e^2) \log\left(\frac{1+e}{1-e}\right) \right\}^{-1} \tag{C.6}$$

$$\alpha_5 = e^2 \left\{ 6e - (3-e^2) \log\left(\frac{1+e}{1-e}\right) \right\}^{-1} \tag{C.7}$$

$$\alpha_4 = 2e^2(1-e^2) \left\{ 2e(3-5e^2) - 3(1-e^2)^2 \log\left(\frac{1+e}{1-e}\right) \right\}^{-1} \tag{C.8}$$

The results for spherical particles can be recovered by noting that

$$\lim_{e \to 0} \alpha_1 = \lim_{e \to 0} \alpha_2 = \frac{3}{8} e^{-1} \tag{C.9}$$

$$\lim_{e \to 0} \gamma = \lim_{e \to 0} \gamma' = \frac{3}{4} e^{-3} \tag{C.10}$$

$$\lim_{e \to 0} \alpha_4 = -\frac{5}{8} e^{-3} \qquad \lim_{e \to 0} \alpha_5 = -\frac{15}{8} e^{-3} \qquad \lim_{e \to 0} \alpha^* = -\frac{5}{4} e^{-3} \tag{C.11}$$

APPENDIX D

Implications of Lorentz' Reciprocal Theorem

Let $\mathbf{u}'$ be the velocity field and $\boldsymbol{\Pi}' = -\mathbf{I}p' + \mu\left(\nabla\mathbf{u}' + (\nabla\mathbf{u}')^T\right)$ be the pressure field corresponding to any flow satisfying the Stokes equations

$$\nabla p = \mu\nabla^2\mathbf{u} \qquad \text{and} \qquad \nabla\cdot\mathbf{u} = 0, \tag{D.1}$$

and let $(\mathbf{u}", \boldsymbol{\Pi}")$ characterize any other fluid motion conforming to (D.1). Then[44]

$$\int_S d\mathbf{S}\cdot\boldsymbol{\Pi}'\cdot\mathbf{u}" = \int_S d\mathbf{S}\cdot\boldsymbol{\Pi}"\cdot\mathbf{u}' \tag{D.2}$$

in which S is any closed suface drawn in the fluid.

This theorem, originally due to Lorentz, defines the symmetry of the resistance tensor of an arbitrary particle.[44–46] It can also be used to determine symmetry requirements for the N-body resistance tensor in systems of particles. Consider for example the two flow cases depicted in fig.9. The velocity field $\mathbf{u}'$ and the associated pressure field $\boldsymbol{\Pi}'$ arise from the motion of a particle "1" with velocity $\mathbf{U}_1$, keeping particle "2" stationary. The fields $\mathbf{u}"$ and $\boldsymbol{\Pi}"$ are caused by spinning particle "2" at an angular velocity $\boldsymbol{\omega}_2$, fixing particle "1". Let the surface S consist of the particle surfaces, and of a shell σ of very large radius R_σ chosen so that σ surrounds both bodies. When applying the reciprocal theorem, the contribution of the outer sphere σ vanishes, since $\boldsymbol{\Pi}'\cdot\mathbf{u}"$ and $\boldsymbol{\Pi}"\cdot\mathbf{u}'$ are at most $O(R_\sigma^{-3})$ as $R_\sigma \to \infty$, while the surface is $O(R_\sigma^2)$. [44] Using the no-slip boundary condition at the particles' surface, we obtain the relation

$$\int_{S_2} d\mathbf{S}\cdot\boldsymbol{\Pi}'\cdot\boldsymbol{\omega}_2\wedge\mathbf{r} = \int_{S_1} d\mathbf{S}\cdot\boldsymbol{\Pi}"\cdot\mathbf{U}_1 \tag{D.3}$$

which can be rearranged as

$$\boldsymbol{\omega}_2\cdot\int_{S_2}\mathbf{r}\wedge\boldsymbol{\Pi}'\cdot d\mathbf{S} = \mathbf{U}_1\cdot\int_{S_1} d\mathbf{S}\cdot\boldsymbol{\Pi}" \tag{D.4}$$

The integral on the left hand side is the hydrodynamic torque experienced by particle "2" under action of the translating particle "1". It depends linearly on $\mathbf{U}_1$ in the limit $Re \to 0$, when the equations (D.1) apply. Hence

$$\int_{S_2} \mathbf{r} \wedge \mathbf{\Pi}' \cdot d\mathbf{S} = \mathbf{R}^{21}_{TU} \cdot \mathbf{U}_1 \tag{D.5}$$

where $\mathbf{R}^{21}_{TU}$ is a crossterm of the resistance matrix for this two-body system. Similarly,

$$\int_{S_1} d\mathbf{S} \cdot \mathbf{\Pi}'' = \mathbf{R}^{12}_{F\omega} \cdot \boldsymbol{\omega}_2 \tag{D.6}$$

is the force experienced by particle "1" due to the rotation of its companion "2". The reciprocal theorem predicts that

$$\boldsymbol{\omega}_2 \cdot \mathbf{R}^{21}_{TU} \cdot \mathbf{U}_1 = \mathbf{U}_1 \cdot \mathbf{R}^{12}_{F\omega} \cdot \boldsymbol{\omega}_2. \tag{D.7}$$

Since $\boldsymbol{\omega}_2$ and $\mathbf{U}_1$ are arbitrary, this implies that

$$\mathbf{R}^{21}_{TU} = (\mathbf{R}^{12}_{F\omega})^T. \tag{D.8}$$

A series of similar expressions can be derived to show that the N-body resistance tensor is symmetric. As mentioned, its invert, the N-body mobility tensor obtained by using the disturbance velocity field (A.16) in the formulae (A.10), (A.14) and (A.15), satisfies this symmetry requirement. This can be recognized by noting that $\mathbf{I}(\mathbf{x})$ is symmetric and that the nabla operator ∇ commutes with integrations.

REFERENCES

1. K.S. Schmitz & J.M. Schurr *J. Phys. Chem.* **76**, 534 (1972).
2. C.R. Cantor & P.R. Schimmel, "Biophysical Chemistry, part II", W.H. Freeman and Company, San Francisco (1980).
3. B.J. Berne & R. Pecora, "Dynamic Light Scattering", John Wiley & Sons, Inc., New York (1976).
4. R.G. Gordon, *J. Chem Phys.* **43**, 1307 (1965).
5. R.G. Gordon, *Adv. Magn. Res.* **3**, 1 (1968).
6. I.D. Kuntz, Jr. & W. Kauzmann, in "Advances in Protein Chemistry" **28**, ed.J C.B. Anfinsen, J.T. Edsall & F.M. Richards, Academic Press, New York and London (1974).
7. J.H. Freed, *J. Chem. Phys.* **41**, 2077 (1964).
8. H.W. Spiess, "NMR basic principles and progress", **15**, Springer, Berlin, Heidelberg & New York (1976).
9. M. Goldman, "Spin Temperature and Nuclear Magnetic Resonance in Solids", Oxford University Press, London (1970).
10. D.E. Woessner, *J. Chem. Phys.* **37**, 647 (1962).
11. W.T. Huntress Jr., *J. Chem. Phys.* **48**, 3524 (1968).
12. A. Einstein, "Investigations on the Theory of the Brownian Motion", Dover Publications Inc., New York (1956).
13. M.J. Perrin, "Brownian Motion and Molecular Reality", Taylor & Francis, London (1910).
14. H. Brenner, *J. Colloid Sci.* **23**, 407 (1967).
15. C.W. Oseen, "Neuere Methoden und Ergebnisse in der Hydrodynamik", Akademische Verlagsgesellshaft, Leipzig (1927).

16. A. Abragam, "Principles of Nuclear Magnetism", Oxford University Press, London (1961).

17. L.D. Favro, *Phys. Rev.* **119**, 53 (1960).

18. L.D. Favro, in "Fluctuation Phenomena in Solids", ed. R.E. Burgess, Academic Press, New York and London (1965), Chapter 3.

19. R.E. London, in "Magnetic Resonance in Biology", ed. J.S. Cohen, J. Wiley & Sons, New York (1980), Chapter 1.

20. L.G. Werbelow & D.M. Grant, *Adv. Magn. Reson.* **9**, 189 (1977).

21. C. Gelfi & P.G. Righetti, *Electrophoresis* **2**, 220 (1981).

22. C. Gelfi & P.G. Righetti, *Electrophoresis* **2**, 213 (1981).

23. H.Y. Carr & E.M. Purcell, *Phys. Rev.***94**, 630 (1954).

24. S. Meiboom & D. Gill, *Rev. Sci. Instr.***29**, 688 (1958).

25. M. Bloom, L.W. Reeves & E.J. Wells, *J. Chem. Phys.***42**, 1615 (1965).

26. S. Arnott, A. Fulmer, W.E. Scott, I.C.M. Dea, R. Moorhouse & D.A. Rees, *J. Mol. Biol.* **90**, 269 (1974).

27. P. Serwer, *Electrophoresis* **4**, 375 (1983).

28. B.D. Hames, in "Gel Electrophoresis of Proteins", ed. B.D. Hames & D. Rickwood, IRL Press, Oxford and Washington D.C. (1981), Chapter 1.

29. G. Bossis & J.F. Brady *J. Chem. Phys.* **80**, 5141 (1984).

30. G. Bossis & J.F. Brady *Ann. Rev. Fluid Mech.* **20**, 111 (1988).

32. P. Mazur & I. Oppenheim, *Physica* **50**, 241 (1970).

32. J. Albers, J.M. Deutch & I. Oppenheim, *J. Chem. Phys.* **54**, 3541 (1971).

33. G. Bossis & J.F. Brady *J. Chem. Phys.* **87**, 5437 (1987).

34. W.B. Russell *Ann. Rev. Fluid Mech.* **13**, 425 (1981).

35. E.J. Hinch *J. Fluid Mech.* **72**, 499 (1975).

36. D.L. Ermak & J.A. McCammon *J. Chem. Phys.* **69**, 1352 (1978).

37. G.J. Kynch *J. Fluid Mech.* **5**, 193 (1959).

38. L. Durlofsky, J.F. Brady & G. Bossis *J. Fluid Mech.* **180**, 21 (1987).

39. D.J. Jeffrey & Y. Onishi *J. Fluid Mech.* **139**, 261 (1984).

40. S.B. Dubin, N.A. Clark & G.B. Benedek *J. Chem. Phys.* **54**, 5158 (1971).

41. A.T. Chwang & T.Y.T. Wu *J. Fluid Mech.* **63**, 607 (1974).

42. A.T. Chwang & T.Y.T. Wu *J. Fluid Mech.* **67**, 787 (1975).

43. S. Kim *Int. J. Multiphase Flow* **11**, 713 (1985).

44. H. Brenner *Chem. Eng. Sci.* **18**, 1 (1963).

45. H. Brenner *Chem. Eng. Sci.* **19**, 703 (1964).

46. E.J. Hinch *J. Fluid. Mech.* **54**, 423 (1972).

47. H. Brenner *Int. J. Multiphase Flow* **1**, 195 (1974).

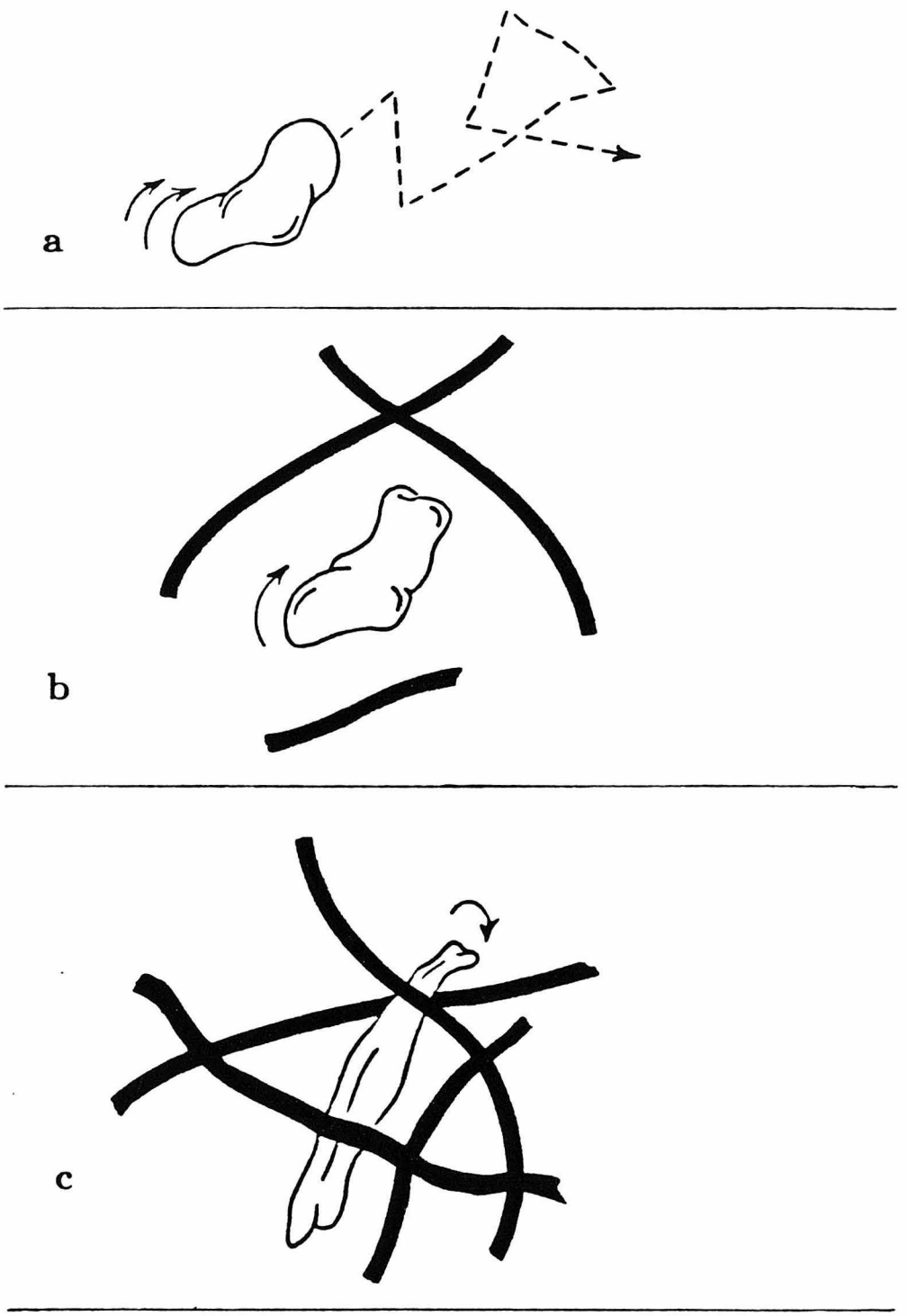

Figure 1 : Effect of entrapment on molecular motion.

a) A particle in an unbounded fluid undergoes translational and rotational Brownian motion.
b) Viscous interactions with the fibers slow the tumbling of the trapped molecule.
c) At high gel concentrations, the anisotropy of the diffusion tensor is amplified because the gel matrix hinders some modes of motion more than others.

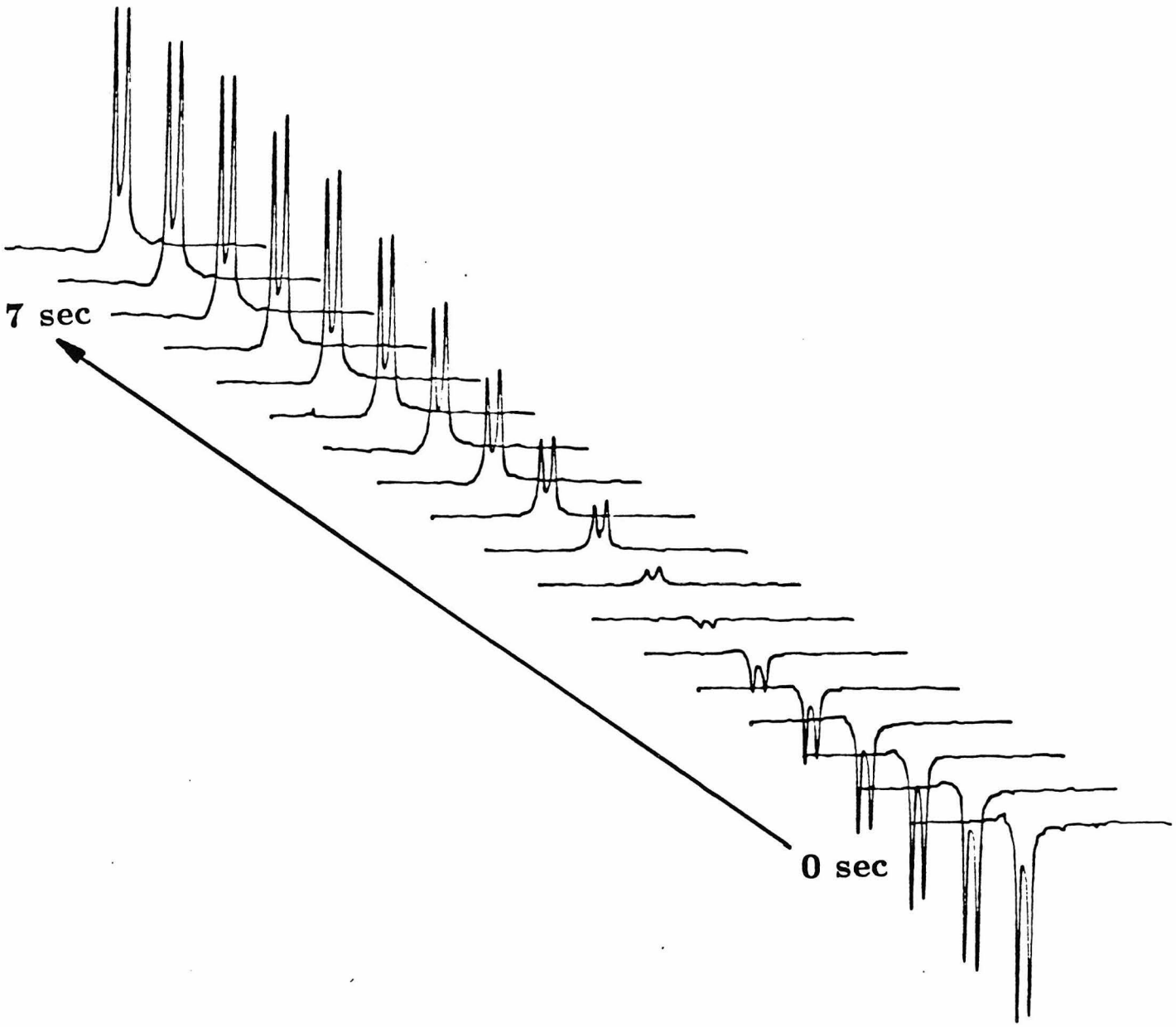

Figure 2 : ^{31}P spin inversion recovery experiment for cyclic guanosine monophosphate in a 50% polyacrylamide gel at a Larmor frequency of 81 MHz. The spectra in this stacked plot were taken at 0.05, 0.1, 0.2, 0.3, 0.45, 0.6, 0.8, 1., 1.25, 1.5, 1.8, 2.2, 2.8, 3.6, 4.6, 5.8, 7., 8.5 seconds after the inverting radiofrequency pulse.

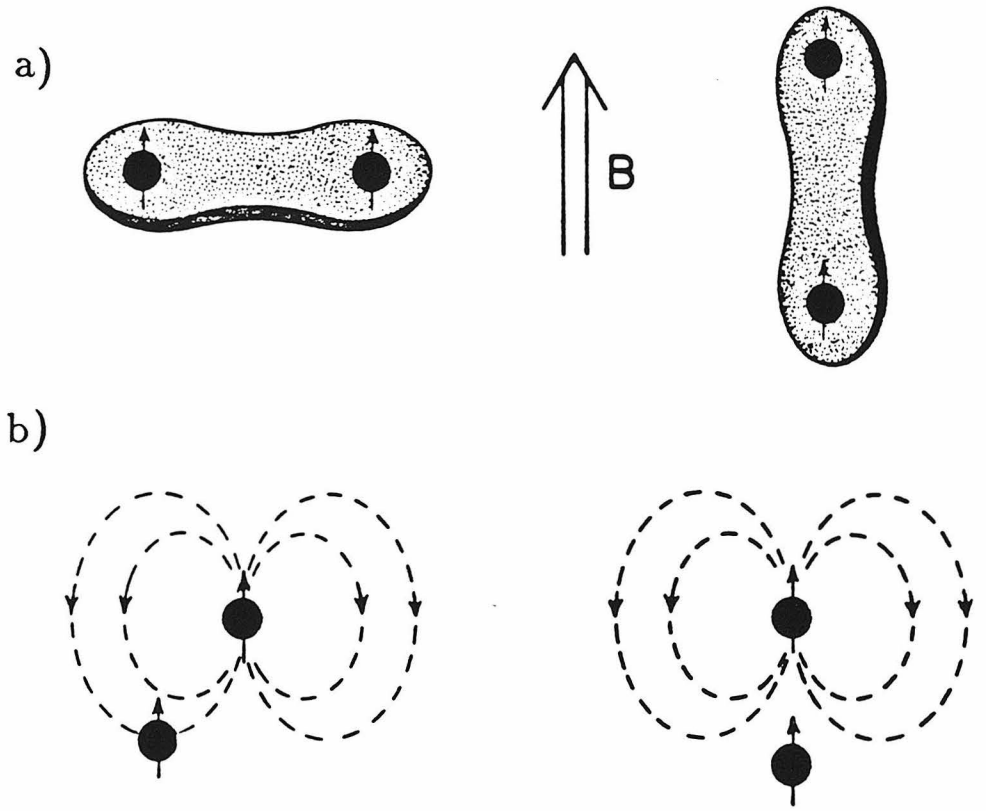

Figure 3 : Influence of molecular orientation on the local magnetic field experienced by the nuclear spins.

a) Illustration of chemical shift anisotropy.

b) Dipole-dipole interaction between nuclear spins.

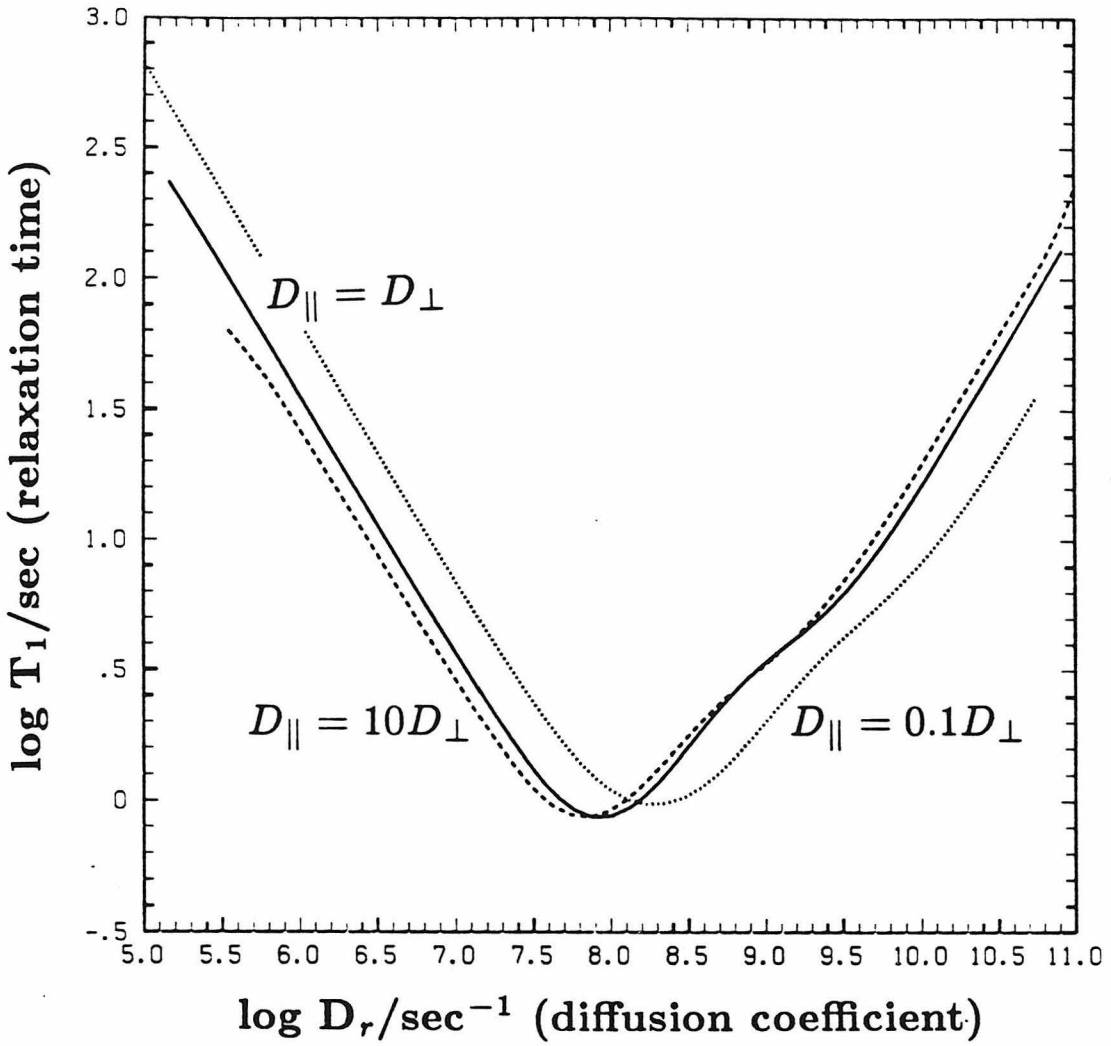

Figure 4 : Double-logarithmic plot of the relaxation time T_1 as a function of the rotational diffusion coefficient $D_r = \frac{1}{3}(D_{||} + 2\,D_{\perp})$. The data are for ^{31}P relaxation at 200 MHz ^1H frequency due to dipole-dipole interaction with a proton 2Å away. The internuclear vector makes an angle of 30° with the major molecular axis (which defines $D_{||}$). The solid line was drawn assuming isotropic diffusion ; the dashed line (---) holds for $D_{||} = 10\ D_{\perp}$ (a prolate body), and the dotted line (...) is for an oblate particle with $D_{||} = 0.1\ D_{\perp}$.

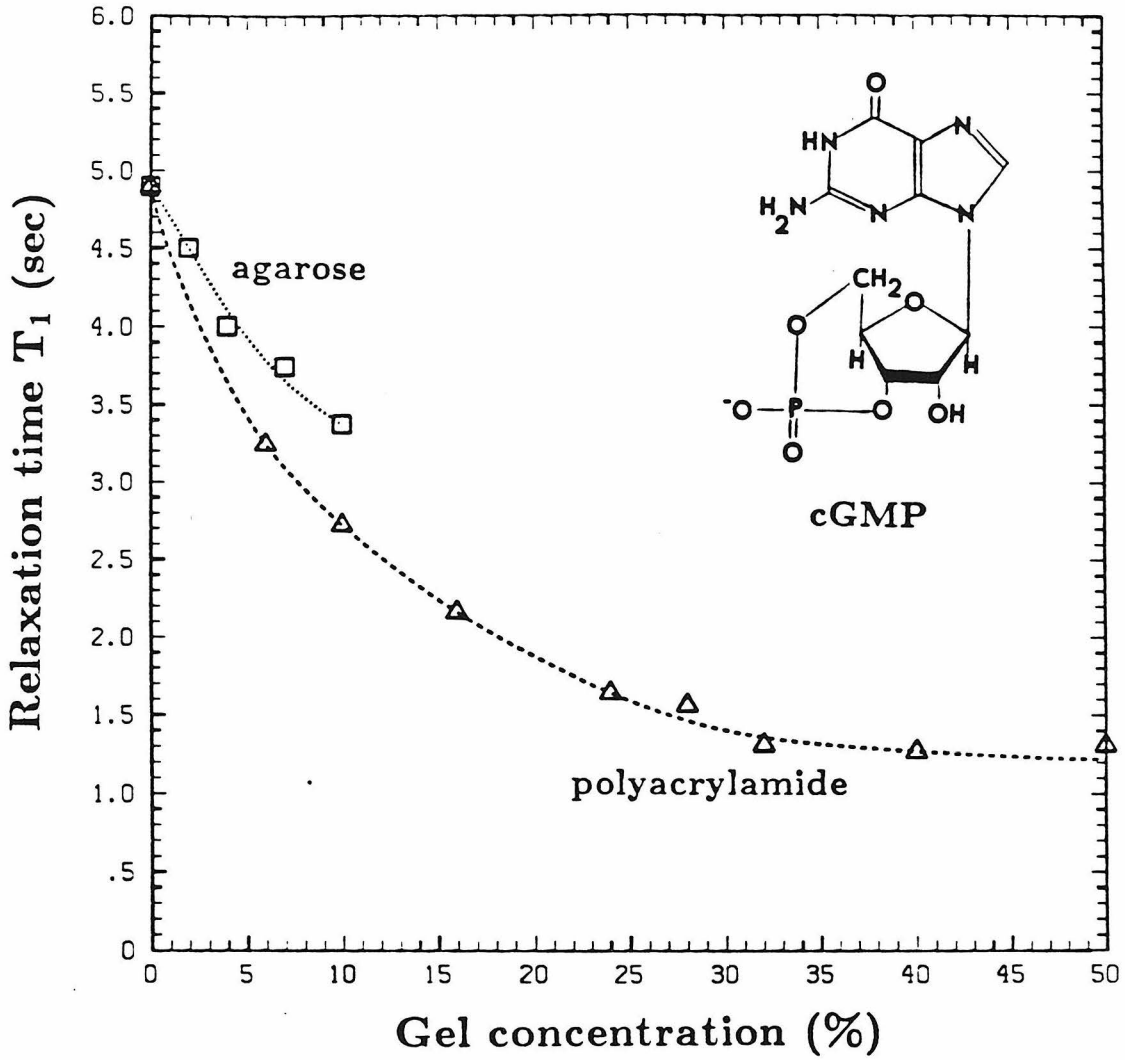

Figure 5 : Experimental results for the ^{31}P relaxation of cGMP in polyacrylamide and agarose gels. The experiments were carried out at room temperature at a Larmor frequency of 80 MHz.

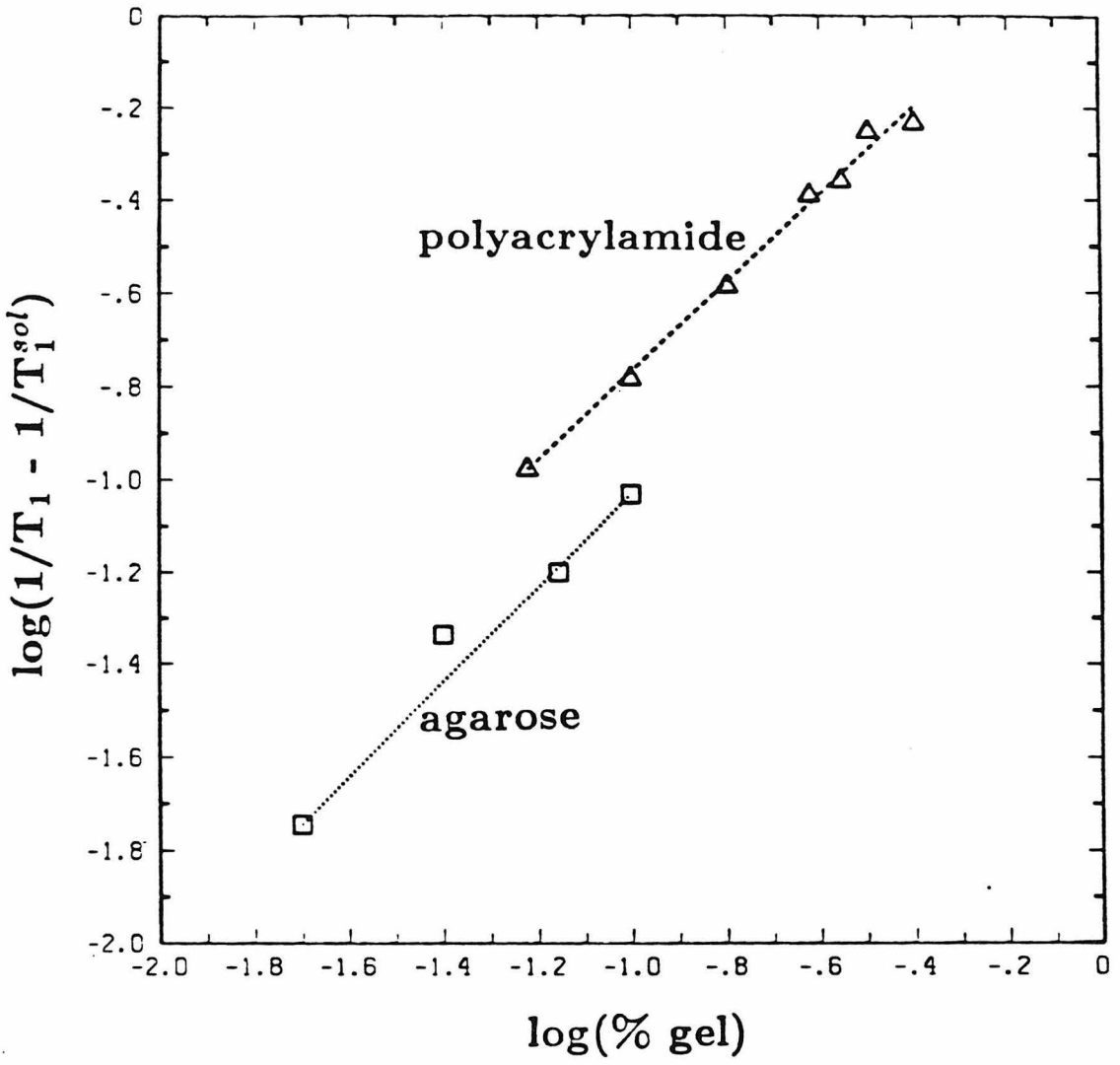

Figure 6 : Double logarithmic diagram of the difference in relaxation rates inside a gel (T_1) and in solution (T_1^{sol}) versus the gel concentration. The data for both gels lie on lines with a slope very close to unity.

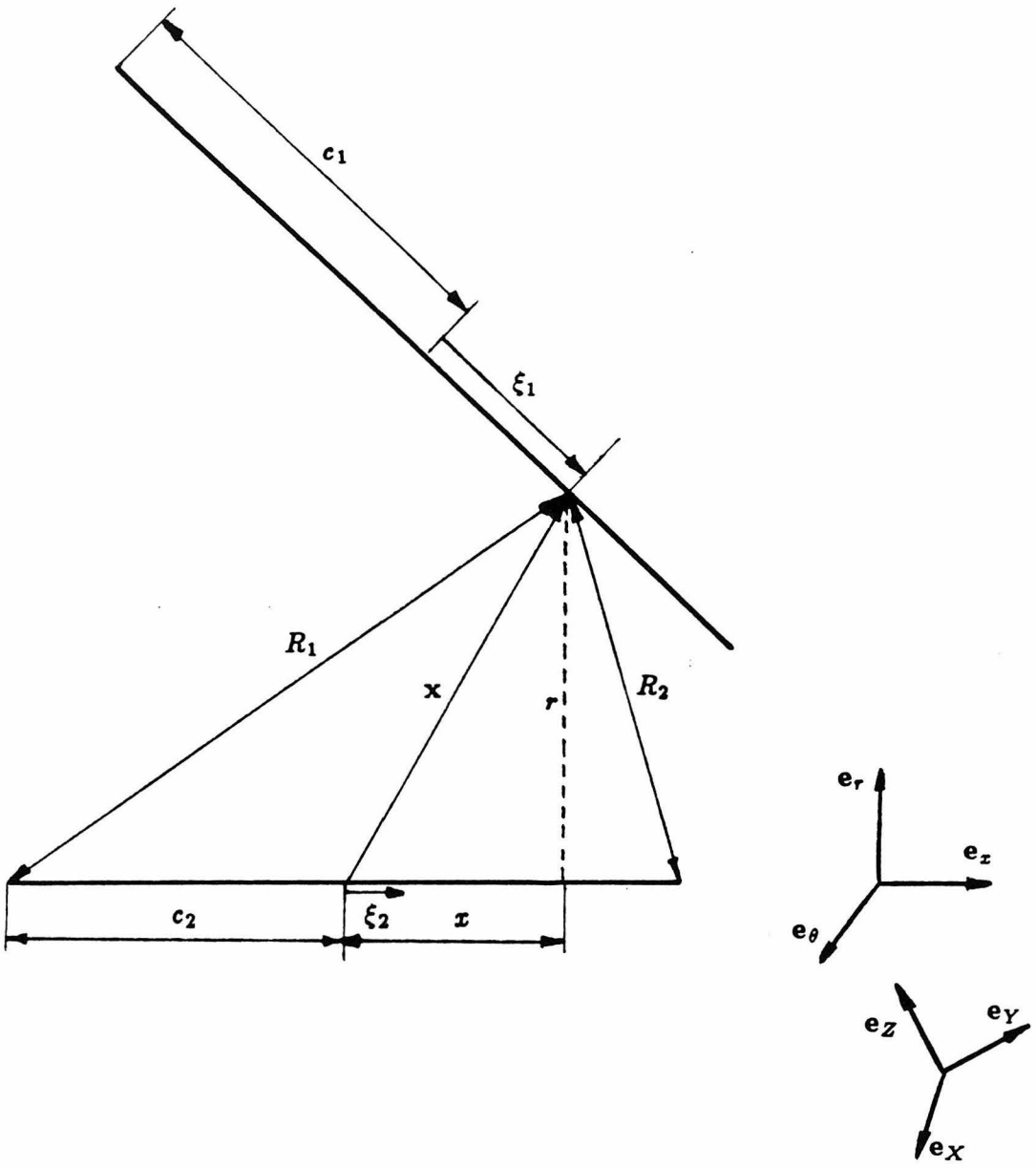

Figure 7 : Local cylindrical coordinates

FLOWCHART FOR CONSTRUCTING THE MOBILITY TENSOR

1. Take particle i 1(1)N-1.
2. Take particle j i+1(1)N.
3. Choose discretization point k. ξ_1 is fixed by k.
4.* Calculate $\{B_{m,n}(\xi_1)\}$.
5.* Calculate the integrand $\mathrm{f}\Big(\{B_{m,n}(\xi_1)\}\Big)$.
6. Transform to laboratory frame of reference.
7.* Integrate numerically using k discretization points.
8. Perform an integral convergence test. If it is not fulfilled, increment k and return to 3.
9. Insert coefficient in mobility matrix.
10. Repeat for next j, starting at 2.
11. Repeat for next i, starting at 1.

The steps marked by an asterisk have been encoded in FORTRAN.

Figure 8: Flowchart for constructing the mobility tensor

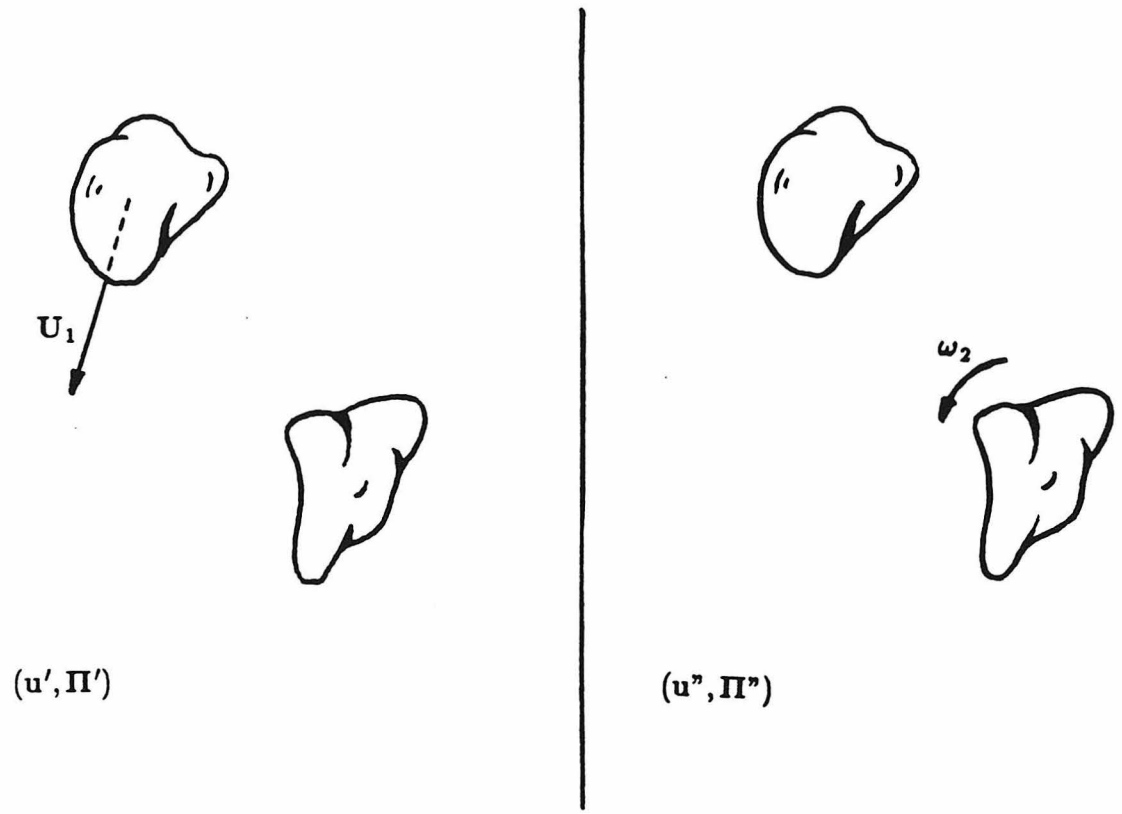

Figure 9 : Flows considered in appendix D